Shape-based Data Analysis for Event Detection in Power Systems

Jose Cordova†, Reza Arghandeh†, Yuxun Zhou*, Stifter Matthias §, Wei Wu‡
†Department of Electrical and Computer Engineering, CAPS, Florida State University
jdc13b@my.fsu.edu
‡Department of Statistics, Florida State University
*Department of Electrical Engineering and Computer Sciences, UC Berkeley
§Energy Department, AIT Austrian Institute of Technology

***Abstract*—Fault classification in power systems is a challenging and complex task due the variety and variability of the electrical parameters of the various network components in spatial and temporal scales. The majority of machine learning methods for event detection require the labeled data sets or examples of previous events. However, the recorded event data happen in different locations, time and system conditions. Therefore, they are not aligned time-series which introduce more challenges for feature selection and signal processing. To perform better feature selection for time-series measurements, shape-based methods along with time alignment (also called registration) are needed. This paper presents the Fisher-Rao Registration Method (FRMM) as a solution for the alignment of different time signals. Amplitude and phase components resulting from the Fisher-Rao registration method provide a means for implementing a hierarchical clustering analysis classifying different fault events by type. The algorithm was tested with the IEEE 13-nodes test feeder simulated in RSCAD environment with over 1500 different fault events presenting an average prediction rate of 98%.**

***Index Terms*—Data Mining, Feature Selection, Shape-based Data Analysis, Event Detection, Power Distribution Networks.**

I. Introduction

The electrical power system is expected to deliver undistorted and uninterrupted sinusoidal rated voltage and current at the rated frequency to the consumers [1]. Deviations and abrupt changes in magnitude and frequency of the voltage and the current signals from the standard rating are treated as a *disturbance* or *fault*, resulting in the risk of malfunction or damaging of electrical and electronic devices [2]. The disturbances are typically caused by equipment failures, human errors and environmental conditions. Power quality (PQ) disturbances and electrical faults followed by cascading effect can increase the risk of outages, given the interconnection and interdependency of the electrical equipment associated with the grid. The multiple levels of abnormal events and the interaction between them make a significant challenge for building high fidelity mathematical models of the systems for fault detection purpose. Therefore, data-driven and modeless tools are needed for detection and classification of electrical faults[1].

Several methodologies consisting of signal processing-based feature extraction along with artificial intelligence based classifiers have proposed to approach this problem. In literature, Neural networks [3], [4], [5] and Support Vector Machines (SVM) [6], [7], [8], [9], [10] are two of the most used methods for classifying power system events such as electrical faults. Many of them are combined with feature extraction methods such as Fast Fourier Transform [10], Wavelet Transform [11], [10], [3], [12], S-transform [6], [13], and Principle Component Analysis (PCA) [8], [14]. One primary concern in these methods is that testing and training data sets are usually not time-aligned, i.e. fault events may happen at any time and any location with different systems conditions during a time window *T*. This introduces inaccuracies and uncertainties in the classification process. In this work, we present a new approach for interpreting, detecting and classifying power system events based on the shape preserving method called the *Fisher-Rao Registration Methods* (FRRM) [15], [16], [17]. Registration has been successfully examined for disturbances classification (e.g. [18]) with simulated signals but not for power systems.

In our approach, we provide a new way of characterizing and measuring distance differences between fault events in a power distribution network. A new notion of distance is used to perform a clustering and to categorize fault types. Based on the distances calculated using the training data, *cluster templates* are created for each type of events. The event templates are then used to construct the proposed shape-based classifier which its performance is evaluated in a cross-validation procedure.

HERE EXPLAIN DIFFERENT SECTIONS OF THE PAPER.

II. Data Shape Preserving based on Fisher-Rao Metric Registration

To explain the concept of the Fisher-Rao Metric Registration (FRRM), consider a set of functions, as shown in Fig. 1a, that differ each other in both height and location of peaks and valleys. Given that they are not aligned with the x axis, a set of warping functions, like the ones depicted in Fig. 1c, must be applied to each original curve so that they become horizontally aligned as shown in Fig. 1b. After using FRRM to a function or a time series (in our case, a voltage or current data stream), the result is an average of all warped functions as shown in Fig. 1d that preserves the shape of the original

data. It will be shown in the following sections that applying a warping function comes from a group action with *composition* as its primary operation.

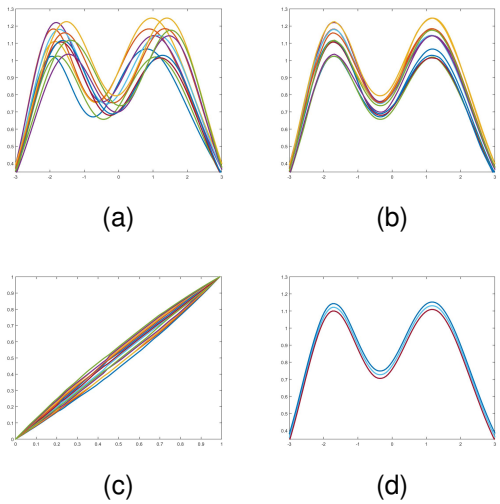

Fig. 1. Fisher-Rao Registration: (a) Set of original data; (b) Data set after alignment or warping; (c) Warping functions; (d) Mean function after warping.

A. Events' Space Construction

The high-resolution monitoring systems based on Phasor Measurement Units (PMUs) and μPMUs that measure three phases of timestamped voltage and current at very high resolution are recently introduced in distribution networks [19]. The typical sampling rate for PMUs is 120 sample per second which is considered as the data frequency in this paper. For the sake of clarity; we will assume for now that every event has the same time span of length T. However, we emphasize that the choice of the time frame in which the data can be analyzed is also itself a non-trivial task. Three phase V and I are defined as follows:

$$\begin{aligned} V &= V(t) : [0,T] \mapsto \mathbb{R}^3 \\ I &= I(t) : [0,T] \mapsto \mathbb{R}^3. \end{aligned} \tag{1}$$

where $V = [V_a(t), V_b(t), V_c(t)]$ and $I = [I_a(t), I_b(t), I_c(t)]$ with $t \in [0,T]$ and T being the length of the event.

In this paper each phase signal corresponds to a different dimension synchronized with timestamps. An event space is defined as a subspace of functions $f : [0,T] \mapsto \mathbb{R}^3$, matched with necessary smoothness and integrability conditions. We will denote the space by $\mathcal{F}$ and the elements of that space, i.e. the signals of fixed length, as $B \in \mathcal{F}$. In our analysis, we are using a newly developed functional data analysis approach to interpreting the events as shapes. Following the shape-based methodology in [15], we are constructing the event shape space (denoted by $\mathcal{S}$) in three steps: First, interpreting the space $\mathcal{F}$ as a Riemannian manifold with the Generalized Fisher-Rao Riemannian metric [20]. Subsequently, transforming $\mathcal{F}$ to a pre-shape space ($\mathcal{S}$) with the Square Root Velocity Function operator denoted by $SRVF(\cdot)$. The elements of $\mathcal{S}$ are then denoted by q as in

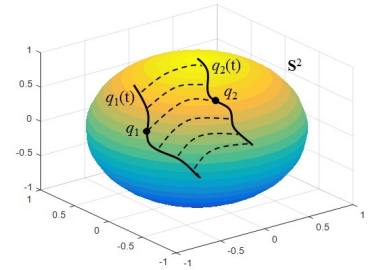

Fig. 2. Distance between shape preserving function q_1 and q_2

$$SRVF(B) = q(t) = \dot{B}(t)/\sqrt{|\dot{B}(t)|}. \tag{2}$$

Finally defining the shape space as a space of equivalence classes of q (denoted by $[q]$) under warpings ($\gamma(t)$) of the time domain of the event. The space from the mathematical point of view is a quotient space S/Γ, where Γ is a set of all domain warping functions $\gamma(t)$.

B. Distances in the Events' Shape Space

The benefit of the SRVF transformation is that it induces a transformation of the Fisher-Rao Riemannian metric to a standard $\mathbb{L}^2$ metric on a sphere.

Define $\mathbb{L}^2([0,1],\mathbb{R})$ (or simply $\mathbb{L}^2$) to be the set of all SRVFs. Then, for every $q \in \mathbb{L}^2$ there exists a function f such that q is the SRVF of that function f.

This has a particular application in the FRRM since warping a function f by γ, then the SRVF of $f \circ \gamma$ becomes:

$$\tilde{q}(t) = (q \circ \gamma)(t)\sqrt{\dot{\gamma}(t)} \tag{3}$$

This transformation will be denoted by $(q,\gamma) = (q \circ \gamma)\sqrt{\dot{\gamma}}$. Following [21] we have that for any two SRVFs q_1, $q_2 \in \mathbb{L}^2$ and $\gamma \in \Gamma$, $\|(q_1,\gamma) - (q_2,\gamma)\| = \|q_1 - q_2\|$. Thus the distance in the space of events can be simply calculated as the arc-length between two points on a sphere. As shown in Fig. 2, the distance between two events $[B_1, B_2]$, which have been transformed to q_1 and q_2 in the sphere $\mathbb{S}^2$ is thus defined as:

$$\begin{aligned} distance_{\mathcal{F}}(B_1,B_2) &= \min_{\gamma} ||q_1 - q_2 \circ \gamma\sqrt{\dot{\gamma}}|| \\ &= \cos^{-1}(< [q_1],[q_2] >_{L^2}). \end{aligned} \tag{4}$$

We will follow the interpretation in the article [15] and denote it the *amplitude distance*. The definition of amplitude distance arises from an intuitive fact that an amplitude difference between two functions should not change upon random, simultaneous domain warpings. In particular: $amplitude(B(t)) = amplitude(B(\gamma(t)))$, where $\gamma : [0,T] \mapsto [0,T]$ is a registration (orientation preserving diffeomorphism). Thus we define an amplitude of a function B as a equivalence class under all time warpings:

$$\begin{aligned} &Amplitude(B) = [B] = \\ &\{B \circ \gamma | \gamma[0,T] \mapsto [0,T], \gamma \in C^{\infty}([0,T])\}. \end{aligned} \tag{5}$$

Algorithm 1 Registration under Fisher-Rao metric

Input: Signals B_i with $i = 1, 2, .., n$.

Output: Amplitude and phase components distances: $distance_{\mathcal{F}}(B_i, B_j)$ and $distance_{phase}(\gamma_{i \to j})$.

Initialisation :

Define $B_i(t) : [0, T] \mapsto \mathbb{R}^3$, $i = 1, 2, ..., n$.
for $i, j = 1, 2, ..., n$. **do**
  Calculate $SRVF(B_i)$ and $SRVF(B_j)$ with (2)
  Calculate $distance_{\mathcal{F}}(B_i, B_j)$ with (4)
  Compute $\gamma_{i \to j}$ with (6)
  Compute $distance_{phase}(\gamma_{i \to j})$ with (7)
end for
return $distance_{\mathcal{F}}(B_i, B_j)$ and $distance_{phase}(\gamma_{i \to j})$

The definition of amplitude difference leaves us with an intuitive approach to the *phase difference*, namely the phase difference reflects the part that is not captured by amplitude. That is the amount of warping γ necessary to align the curve B_1 to B_2 after the SRVF transformation, to minimize the amplitude-distance between them. It is worth mentioning that the amplitude and phase in this context are geometrical parameters of mapped data point on the sphere space, not to be confused with the electric voltage and current phasor values.

The optimal γ is found using the dynamic programming approach with the use of an R [22] package "fdasrvf" [23]:

$$\gamma_{1 \to 2} = arg \min_{\gamma} d_{SRVF}(q_1, q_2 \circ \gamma \sqrt{\dot{\gamma}}). \tag{6}$$

where γ represents the phase adjustment. This can be quantified as follows:

$$distance_{phase}(\gamma_{1 \to 2}) = \cos^{-1}(< 1, \sqrt{\dot{\gamma}_{1 \to 2}} >). \tag{7}$$

Hence, for every signal B_1 and B_2, two distances will be calculated as result after the FRRM: the $distance_{\mathcal{F}}(B_1, B_2)$ and the $distance_{phase}(\gamma_{1 \to 2})$. The FRRM is resumed in algorithm 1.

III. The Case-study for High Resolution Measurement Data

A. RSCAD model of IEEE 13 Test Feeder

Fig. 3 shows the IEEE 13 nodes test feeder used as a case of study for this paper. The test feeder is highly loaded for a 4.16 kV system and presents the inherent high unbalance of a normal distribution network. The complete data used for this system may be found in [24].

In order to validate the effectiveness of the FRRM-based classification algorithm, a set of fault events were applied to the test feeder. The test feeder is implemented in RSCAD. Different faults with a duration of 0.2 seconds (approx. 12 cycles) were applied, one at a time, in three locations: nodes 645, 680, and 692 (see Fig. 3).

Measurements from the distribution test feeder are necessary for the fault type classification algorithm. In a distribution network, it is usual that only the main feeder has a measurement device providing voltage and current time-series. For this test case, the meter providing both voltage and current readings is located at node 632, that is, the secondary side of the main feeder's transformer (see Fig. 3).

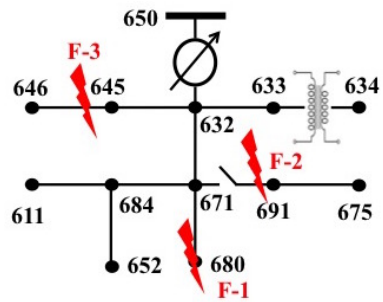

Fig. 3. Imposed fault locations on the IEEE 13 nodes test feeder [24]

TABLE I
Labeling by Fault Type

Labels	
4 fault-types labels	11 fault-types labels
AG, BG, CG	SPH (Single-phase)
ABG, BCG, ACG	2PHG (Two-phase-to-ground)
AB, BC, AC	2PH (Two-phase)
ABCG, ABC	3PH (Three-phase)

In a three phase system, there are eleven types of faults possible which include phase A to ground (AG), phase B to ground (BG), phase C to ground (CG), phases A & B to ground (ABG), phases B & C to ground (BCG), phases A & C to ground (ACG), phase A to phase B (AB), phase A to phase C (AC), phase B to phase C (BC), three-phase (ABC), and three-phase-to-ground (ABCG). For each fault type, a total of 50 events were simulated with random low impedance values ranging from 0.01 to 0.015 ohm. A set of 550 training/test observations of these bolted faults were simulated for each location, giving a total of 1650 analyzed fault events. Additionally, in order to test the FRRM, a re-categorization of fault type classes has been assigned as shown in table I.

Three events are presented here as an example: Fig. 4a shows a single-line-to-ground fault as seen from the meter (node 632), showing that voltage from the faulted phase decreasing considerably while the current increases to dangerous levels in the same phase. Double-line-to-ground and three-phase fault types present the same behavior for two and three phases respectively (see Fig. 4b and Fig. 4c).

IV. Validation & Discussion

A. Clustering and Categorizing

As stated in section II, the FRRM algorithm returns the amplitude and phase components distances, $distance_{\mathcal{F}}(B_i, B_j)$ and $distance_{phase}(\gamma_{i \to j})$, for an n number of signals. This results in a nxn matrix where its elements represent the distance between its components. The matrix containing these distances

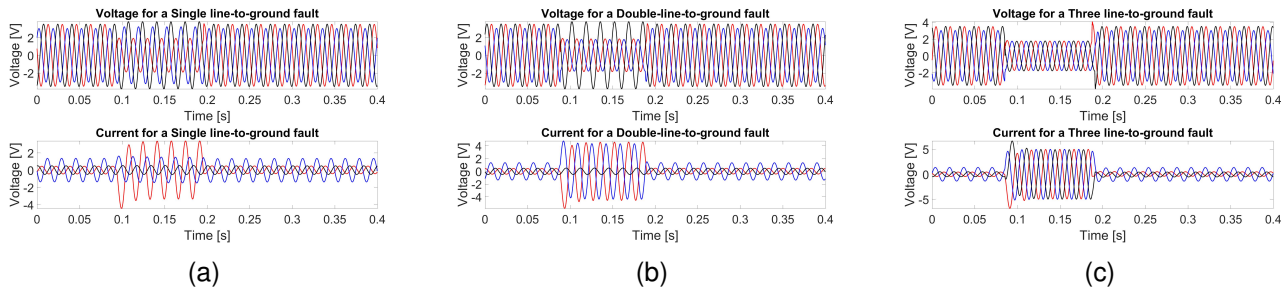

Fig. 4. **RSCAD simulations of IEEE 13 nodes test feeder**: (a) Measurements from node 632 with a single-line-to-ground fault at node 680; (b) Measurements from node 632 with a double-line-to-ground fault at node 680; (c) Measurements from node 632 with a three-phase fault at node 680;

provides the necessary information to perform a classification algorithm by clustering similar events or observations by their fault types. It is important to remark that in a real power system, most of the different fault events will not have a label providing their type. Therefore, an unsupervised learning method, such as Hierarchical Clustering, provides a more realistic approach to the classification problem. For our case of study, knowing the fault type (or class) of each event simulated will provide a metric to determine the prediction accuracy of our classification algorithm.

Hierarchical cluster analysis (HCA) seeks to build a hierarchy of clusters based on the distances between each of the observations being classified. Each fault type has been given a class and it is expected that after applying the FRRM, events with the same label have similar distance values.

Fig. 5 shows the result of the FRRM for each one of the fault locations. For the faults simulated at node 680, the multidimensional scaling (MDS) visualization for 11 fault-type labels, the re-categorization of 4 fault-type labels and the resulting clustering matrix are shown in figures 5a, 5b and 5c respectively. The same resulting plots are shown for nodes 692 and 645 in the second and third row of Fig. 5 respectively.

Fig. 5a shows the MDS representation of the FRRM resulting matrix for node 680. MDS is a technique to visualize the information contained in a distance matrix while preserving the between-object distances as much as possible. In this figure, it can be seen that different types of faults tend to cluster in this MDS representation. There is a large clustering for single-line-to-ground faults which are distributed in the center of plot while two-phase and three-phase are distributed in the left and right respectively. The re-categorized fault types are shown in Fig. 5b. This figure shows again the single-phase events in the center while the two-phase and three-phase faults are distributed in the left and right respectively. Fig. 5c presents the clustering matrix for the faults set at node 680. The clustering matriz contains the distances resulting from the FRRM between each pair of signals. A small distance value means that the signals are similar. Thus, it is likely that signals from an specific fault type have small distances difference, clustering together. As expected, the diagonal in the clustering matrix shows a group of events having similar distances, showing that there is a representative clustering by fault types.

Fig. 5d shows the MDS visualization for the faults set at node 692. Faults at this node present a similar pattern as at node 680, with three-phase events clustering on the left side of the plot as they present similar distance values. Single-phase faults are grouped in the in the center while two-phase faults are gathered on the right. The 4-fault-types labels confirm these clustering pattern as seen in Fig. 5e. Also, the clustering matrix (Fig. 5f) presents the group patterns as a result of the hierarchical clustering, where similar distance values can be seen across the diagonal.

The faults taking place at node 645 present a remarkable difference with respect to the previous to faulted nodes. Fig. 5g shows a distinctive clustering for three-phase faults in the top left, two-phase faults on the right while single-phase events are shown in bottom-center section of the MDS plot. This distinction can be seen more clearly in Fig. 5h, showing that the algorithm was able to distinguish the number of faulted phases in a very accurate manner. The clustering matrix in Fig. 5i shows three marked clusters across the diagonal, validating the visualization with respect to the labels. Observing Fig. 3, it can be seen that node 645 is directly next to the node where the meter is located. Therefore, it becomes expected that the best clustering is performed in nodes closer to the meter.

B. Cross-Validation for Clustering

The nature of unsupervised learning methods such as HCA draws up a big challenge for testing its prediction accuracy. It becomes essential to have a training and a testing set with defined labels to measure if the algorithm is clustering into the classes needed. In order to obtain the prediction rate of the HCA-FRRM, a cross validation technique was utilized. A large number of observations were sampled from the fault set and used as a test while the remaining performed as a training set to predict the event class. A nearest-neighbor approach was taken in order to determine the class to which the observed event belongs. Results from the cross-validation method are shown in table II. Prediction with 4-fault-type labels has very high accuracy with an average of 98.9% prediction rate. For the 11-fault-type labels, the prediction rate has an average of 78.33%. Once again, location 3 has the best prediction from among the three locations used as the meter is closer to this

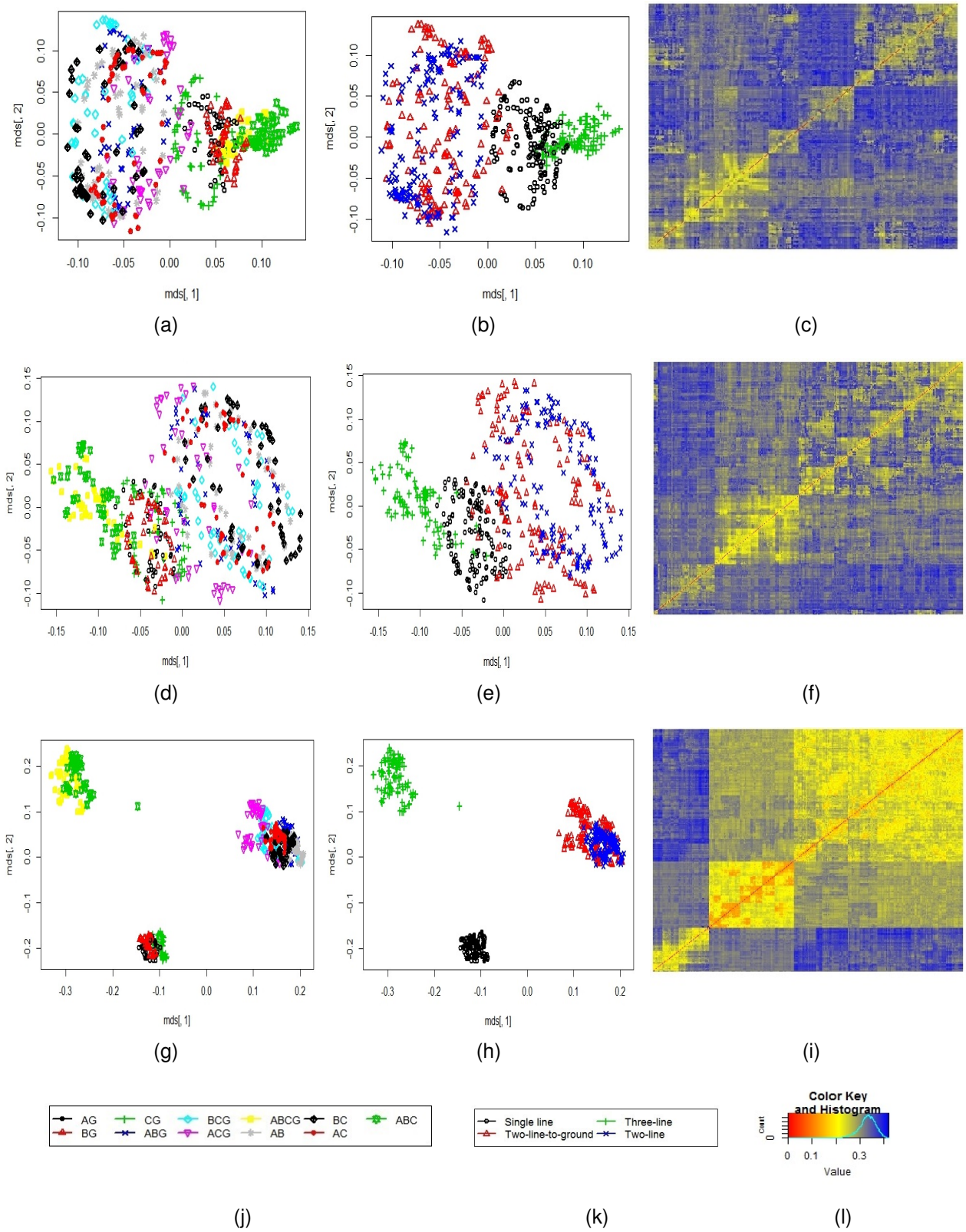

Fig. 5. **Clustering for Voltage - Amplitude distances**: (a) 11 fault types applied to node 680 (550 observations); (b) 4 fault types applied to node 680 (550 observations); (c) Clustering matrix for node 680; (d) 11 fault types applied to node 692 (550 observations); (e) 4 fault types applied to node 692 (550 observations); (f) Clustering matrix for node 692. (g) 11 fault types applied to node 645 (550 observations); (h) 4 fault types applied to node 645 (550 observations); (i) Clustering matrix for node 645. (j) Legend for 11-fault-type labels. (k) Legend for 4-fault-type labels. (l) Distance value color code.

node. This infers that the location of the meter is crucial for having a high prediction rate.

TABLE II
FAULT CLASSIFICATION PREDICTION RATE

Location	Labels	
	4 fault-types labels	11 fault-types labels
Node 680	98.3%	81.3%
Node 692	98.6%	70.69%
Node 645	100%	83%

C. Future Work

Further steps and our future direction which didn't fit into the scope of this paper are as follow. Other methods of exhaustive and non-exhaustive cross-validation methods such as "Leave-p-out" and "k-fold" will be used to test the prediction rate further. The algorithm will also be validated with other unsupervised learning techniques such as centroid-based and distribution-based clustering. Instead of comparing a signal with the every signal of the training set, characteristic templates of the different types of faults will be created with FRRM for direct comparison. The optimal placement of the measuring devices can lead to better result as it was seen that the clustering is strongly related to the location as the fault impedance seen from the metering device changes.

V. CONCLUSIONS

In this paper, a classification method based on the Fisher-Rao registration was presented. Amplitude and phase distances between signals are used to cluster them into their fault types. Over 1500 fault types were simulated in RSCAD to test the algorithm. After applying the FRRM, events with the same class tended to cluster together, as expected. It was seen that nodes 692 and 680 had a similar pattern, where it was distinguishable what type of event was taking place. Faults set at node 645 had a particular behavior as the clustering was more clearly defined. This was expected as node 645 is closer to the metering device which infers that the algorithm would perform better with an optimal metering allocation. A cross-validation method was implemented to determine the algorithm's performance showing a 98% of average accuracy for a number of phases faulted prediction as shown in table II. Prediction for faulted phases had an average of 78% of prediction rate.

ACKNOWLEDGMENT

This research is sponsored in part by the U.S. NSF award 1640587.

REFERENCES

[1] N. G. O. Mahela, A. Shaik, "A critical review of detection and classification of power quality events," *Renewable and Sustainable Energy Reviews*, 2014.

[2] I. Y. G. Math H.J. Bollen, *Signal Processing of Power Quality Disturbances*. New Jersey: IEEE Press, 2005.

[3] D. G. Cesar, V. G. Valdomiro, and O. P. Gabriel, "Automatic power quality disturbances detection and classification based on discrete wavelet transform and artificial intelligence," in *Transmission Distribution Conference and Exposition: Latin America, 2006. TDC '06. IEEE/PES*, Aug 2006, pp. 1–6.

[4] K. M. Silva, B. A. Souza, and N. S. D. Brito, "Fault detection and classification in transmission lines based on wavelet transform and ann," *IEEE Transactions on Power Delivery*, vol. 21, no. 4, pp. 2058–2063, Oct 2006.

[5] M. Valtierra-Rodriguez, R. de Jesus Romero-Troncoso, R. A. Osornio-Rios, and A. Garcia-Perez, "Detection and classification of single and combined power quality disturbances using neural networks," *IEEE Transactions on Industrial Electronics*, vol. 61, no. 5, pp. 2473–2482, 2014.

[6] S. Ekici, "Classification of power system disturbances using support vector machines," *Expert Systems with Applications*, vol. 36, no. 6, pp. 9859 – 9868, 2009. [Online]. Available: http://www.sciencedirect.com/science/article/pii/S0957417409001389

[7] G. Lv, X. Wang, H. Zhang, and C. Zhang, "Pq disturbances identification based on svms classifier," in *Neural Networks and Brain, 2005. ICNN B '05. International Conference on*, vol. 1, 2005, pp. 222–226.

[8] Y. Zhou, R. Arghandeh, and A. v. M. I. Konstantakopoulos, S. Abdullah, "Abnormal event detection with high resolution micro-pmu data," *19th Power Systems Computation Conference*, 2016.

[9] Y. Zhou, R. Arghandeh, and C. J. Spanos, "Online learning of contextual hidden markov models for temporal-spatial data analysis," *2016 IEEE Control Systems Society Conference Management System (CDC 2016)*, 2016.

[10] D. Srinivasan, W. S. Ng, and A. C. Liew, "Neural-network-based signature recognition for harmonic source identification," *IEEE Transactions on Power Delivery*, vol. 21, no. 1, pp. 398–405, Jan 2006.

[11] A. K. Chandel, G. Guleria, and R. Chandel, "Classification of power quality problems using wavelet based artificial neural network," in *Transmission and Distribution Conference and Exposition, 2008. IEEE/PES*, 2008, pp. 1–5.

[12] W. M. Lin, C. H. Wu, C. H. Lin, and F. S. Cheng, "Detection and classification of multiple power-quality disturbances with wavelet multiclass svm," *IEEE Transactions on Power Delivery*, vol. 23, no. 4, pp. 2575–2582, 2008.

[13] S. R. Samantaray, "Decision tree-initialised fuzzy rule-based approach for power quality events classification," *IET Generation, Transmission Distribution*, vol. 4, no. 4, pp. 530–537, April 2010.

[14] Y. Chen, L. Xie, and P. R. Kumar, "Power system event classification via dimensionality reduction of synchrophasor data," in *2014 IEEE 8th Sensor Array and Multichannel Signal Processing Workshop (SAM)*, June 2014, pp. 57–60.

[15] A. Srivastava, W. Wu, S. Kurtek, E. Klassen, and J. Marron, "Statistical analysis and modeling of elastic functions," *arXiv preprint arXiv:1103.3817*, 2011.

[16] J. D. Tucker, W. Wu, and A. Srivastava, "Generative models for functional data using phase and amplitude separation," *Computational Statistics & Data Analysis*, vol. 61, pp. 50–66, 2013.

[17] A. Srivastava, E. Klassen, S. H. Joshi, and I. H. Jermyn, "Shape analysis of elastic curves in euclidean spaces," *IEEE Transactions on Pattern Analysis and Machine Intelligence*, vol. 33, no. 7, pp. 1415–1428, 2011.

[18] A. M. Youssef, T. K. Abdel-Galil, E. F. El-Saadany, and M. M. A. Salama, "Disturbance classification utilizing dynamic time warping classifier," *IEEE Transactions on Power Delivery*, vol. 19, no. 1, pp. 272–278, Jan 2004.

[19] A. von Meier, D. Culler, A. McEachern, and R. Arghandeh, "Micro-synchrophasors for distribution systems," in *Innovative Smart Grid Technologies Conference (ISGT), 2014 IEEE PES*, Feb 2014, pp. 1–5.

[20] E. P. K. Anuj Srivastava, *Functional and Shape Data Analysis*. New York: Springer-Verlag New York, 2016.

[21] A. Srivastava, W. Wu, S. Kurtek, E. Klassen, and J. Marron, "Registration of functional data using fisher-rao metric," *arXiv preprint arXiv:1103.3817*, 2011.

[22] R Core Team, *R: A Language and Environment for Statistical Computing*, R Foundation for Statistical Computing, Vienna, Austria, 2015. [Online]. Available: https://www.R-project.org/

[23] J. D. Tucker, *fdasrvf: Elastic Functional Data Analysis*, 2016, r package version 1.6.1. [Online]. Available: https://CRAN.R-project.org/package=fdasrvf

[24] W. H. Kersting, “Radial distribution test feeders,” in *Power Engineering Society Winter Meeting, 2001. IEEE*, vol. 2, 2001, pp. 908–912 vol.2.